

Experimental realization of fractal fretwork metasurface for sound anomalous modulation

Jiajie He, Shumeng Yu, Xue Jiang, and Dean Ta

Citation: Chin. Phys. B, 2024, 33 (**5**): 054301. DOI: 10.1088/1674-1056/ad2dcd
Journal homepage: http://cpb.iphy.ac.cn; http://iopscience.iop.org/cpb

What follows is a list of articles you may be interested in

Sensing the heavy water concentration in an H_2O—D_2O mixture by solid—solid phononic crystals

Mohammadreza Rahimi and Ali Bahrami
Chin. Phys. B, 2024, 33 (**4**): 044301. DOI: 10.1088/1674-1056/ad0bf5

Reconfigurable source illusion device for airborne sound using an enclosed adjustable piezoelectric metasurface

Yi-Fan Tang(唐一璠) and Shu-Yu Lin(林书玉)
Chin. Phys. B, 2023, 32 (**3**): 034306. DOI: 10.1088/1674-1056/ac9fc0

Controlling acoustic orbital angular momentum with artificial structures: From physics to application

Wei Wang(王未), Jingjing Liu(刘京京), Bin Liang (梁彬), and Jianchun Cheng(程建春)
Chin. Phys. B, 2022, 31 (**9**): 094302. DOI: 10.1088/1674-1056/ac7868

Manipulation of acoustic wavefront by transmissive metasurface based on pentamode metamaterials

Ying Liu(刘颖), Yi-Feng Li(李义丰), Xiao-Zhou Liu(刘晓宙)
Chin. Phys. B, 2019, 28 (**2**): 024301. DOI: 10.1088/1674-1056/28/2/024301

Bidirectional asymmetric acoustic focusing with two flat acoustic metasurfaces

Di-Chao Chen(陈帝超), Xing-Feng Zhu(朱兴凤), Qi Wei(魏琦), Da-Jian Wu(吴大建)
Chin. Phys. B, 2018, 27 (**12**): 124302. DOI: 10.1088/1674-1056/27/12/124302

Experimental realization of fractal fretwork metasurface for sound anomalous modulation

Jiajie He(何佳杰)[1], Shumeng Yu(于书萌)[1], Xue Jiang(江雪)[1,†], and Dean Ta(他得安)[1,2,‡]

[1] *Department of Biomedical Engineering, School of Information Science and Technology, Fudan University, Shanghai* 200433, *China*
[2] *Academy for Engineering and Technology, Fudan University, Shanghai* 200433, *China*

(Received 15 January 2024; revised manuscript received 24 February 2024; accepted manuscript online 28 February 2024)

Natural creatures and ancient cultures are full of potential sources to provide inspiration for applied sciences. Inspired by the fractal geometry in nature and the fretwork frame in ancient culture, here we design the acoustic metasurface to realize sound anomalous modulation, which manifests itself as an incident-dependent propagation behavior: sound wave propagating in the forward direction is allowed to transmit with high efficiency while in the backward direction is obviously suppressed. We quantitatively investigate the dependences of asymmetric transmission on the propagation direction, incident angle and operating frequency by calculating sound transmittance and energy contrast. This compact fractal fretwork metasurface for acoustic anomalous modulation would promote the development of integrated acoustic devices and expand versatile applications in acoustic communication and information encryption.

Keywords: acoustic metasurface, fractal geometry, sound anomalous modulation

PACS: 43.20.+g, 43.28.+h **DOI:** 10.1088/1674-1056/ad2dcd

1. Introduction

Fractal is glowing with new vitality in multidisciplinary sciences, including mathematics, physics, biomimetic materials, and geology.[1–5] Fractal geometry exhibits a high degree of self-similarity on different scales, which is inspired by the unique structures in nature such as snowflakes, ferns, and nautiluses. Due to the self-similar property, fractal architectures manifest hierarchical physical responses arising from the synergism of multiple units, while maintaining the behavior of each individual unit.[6–10] Diverging surface areas within a finite volume is conducive to construct the ultra-deep subwavelength configurations and develop the integrated miniaturized devices. Besides the wisdom from natural creatures, one can also learn from the intelligence in ancient cultures such as the origami which has spurred diverse applications in mechanical engineering, robots design, and computational algorithm.[11–13] Another elegant ancient art is the fretwork frame. It refers to a traditional decorative pattern folded horizontally and vertically to form a "square convolute" shape, which is prevalent in ancient pottery, bronze, jade, and architectural ornaments for continuous good fortune. The spatial convolute geometry is derived from the vortex generated by water flow and has been introduced into acoustics to extend the propagation path of sound wave, exciting important applications in sound manipulation.[14–17]

Ongoing developments of acoustic metasurfaces have opened up new avenues to realize sound anomalous modulation. Metasurfaces with specially designed artificial microstructures can remarkably modulate sound wave. Extraordinary abnormal transmission previously inconceivable has been achieved, including sound cloaking,[18–20] hologram,[21,22] super-resolution focusing,[23,24] and insulation.[25–27] Asymmetric transmission,[28–31] which solely allows sound wave to be travelling in one direction and strongly decreased in the opposite direction, enabling an incident-dependent functionality and extraordinary potentials in acoustic communication and information encryption. Although relevant works have provided useful strategies to realize asymmetric manipulation based on the complex active systems or passive structures,[32–42] new design schemes are still highly desired for the more robust unidirectional transmission with compact subwavelength structures.

2. Metasurface design

We introduce the multi-scale self-similar fractal models to design acoustic metasurface, based on the fundamental architecture frame of the fretwork pattern, as schematically depicted in Fig. 1(a). The fractal fretwork meta-atom occupies compact space due to the shrinkage size of fractal hierarchy and inward rotation of fretwork pattern to increase the path length of sound transmission. The comparison of sound pressure fields for acoustic anomalous modulation is presented in Fig. 1(b). For the normal transmission (left panel), sound wave penetrates both from the front (red arrows) and rear (blue arrows) sides, obeying the reciprocity principle. However, sound wave can only transmit in the forward guidance and almost entirely blocked in the opposite guidance for the abnormal transmission (right panel). This incident-dependent propagation constitutes a selective on/off state control over the wave energy flow.

†Corresponding author. E-mail: xuejiang@fudan.edu.cn
‡Corresponding author. E-mail: tda@fudan.edu.cn

© 2024 Chinese Physical Society and IOP Publishing Ltd

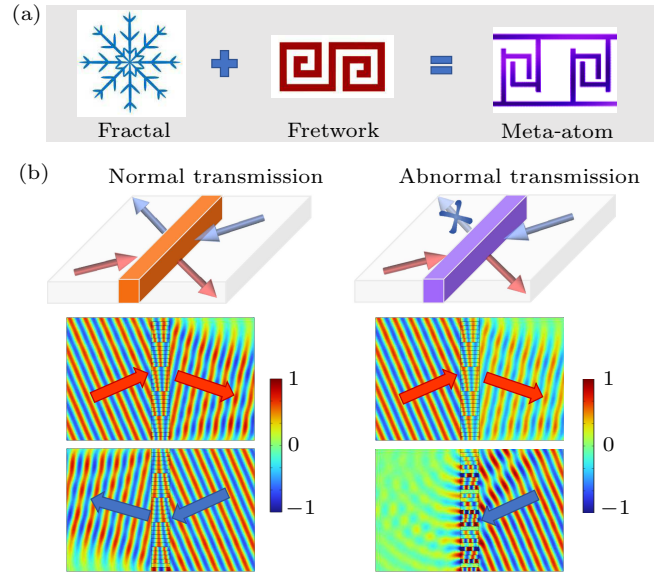


Fig. 1. Schematic diagram of the fractal fretwork metasurface for acoustic anomalous modulation. (a) Design concept of the acoustic meta-atom inspired by the fractal geometry and fretwork frame. (b) Comparison of sound fields in the normal (left) and abnormal (right) transmissions.

Recently, the inherent viscosity loss has been incorporated in asymmetric transmission as a new degree of freedom to design acoustic diodes and chiral exceptional point.[35,43] Diffraction of the metasurface is affected by the interplay of phase gradient and structure period, following the generalized Snell's law:[44,45] $k_0(\sin\theta_t - \sin\theta_i) = 2\pi m/L = \mathrm{d}\Phi/\mathrm{d}x + (m-1)G$. Here, k_0 is the sound wave vector in air, θ_i and θ_t are the incident and transmit angles, respectively. m is the diffraction order and L is the structure periodicity. Both the phase gradient $\mathrm{d}\Phi/\mathrm{d}x$ and the reciprocal lattice vector G are $2\pi/L$ in our configuration. Then, the x and z components of sound wave vector in the m-th order diffraction are represented as $G_m = k_x + 2\pi m/L$ and $k_{z,m} = \sqrt{k_0^2 - G_m^2}$, where k_x is the incident wave vector in x direction.[46] Only the modes of real value $k_{z,m}$ are allowed to propagate, that is $k_{z,m}^2 > 0$ $(k_0^2 - G_m^2 > 0)$. Therefore, we can obtain that the dominant propagating modes of sound are $m = +1$ in the forward direction and $m = -1$ in the backward direction.[47]

Three-dimensional (3D) geometry structures of the meta-atom with the first, second, and third orders are illustrated in Fig. 2(a). The width and length of each meta-atom are standardized as $a = 20$ mm and $b = 100$ mm, and the layer thickness within the meta-atom is $w = 1$ mm. The layer height h_1 is adjustable to control the phase delay in the structure, and other distances between the layers are fixed to be $d = 8$ mm and $l = 3$ mm. The evolution of higher-order meta-atoms is proportionally replicated from the lower-order meta-atoms by the fractal scale factor. In order-1 structure, the fractal scale factor is selected as the ratio $\alpha = h_1/(h_1 + l)$. In order-2 structure, new layers with the height of h_2 are scaled down via the fractal scale factor $\alpha = h_2/(d - w)$ and bend inward at the position $m = \alpha h_1$ to construct the self-similar geometry. Similarly, in order-3 structure, the height of new layers h_3 is obtained by $\alpha = h_3/(2m - h_1 - l)$, with the bending position of $n = \alpha h_2$. The effective propagation length of sound wave passing through the meta-atoms becomes extended and circuitous with the increase of fractal orders. We summarize the relationships between the phase/transmittance and the structure parameter h_1 in different hierarchical orders. For obtaining a phase interval of $\pi/3$ with high transmittance, the meta-atoms of $h_1 = 5.5$ mm, $h_1 = 9.4$ mm, and $h_1 = 13.6$ mm in order-1 structures, $h_1 = 13.4$ mm and $h_1 = 14.8$ mm in order-2 structures, and $h_1 = 14.9$ mm in order-3 structures are selected to construct the metasurface, as denoted by the solid markers in Fig. 2(b).

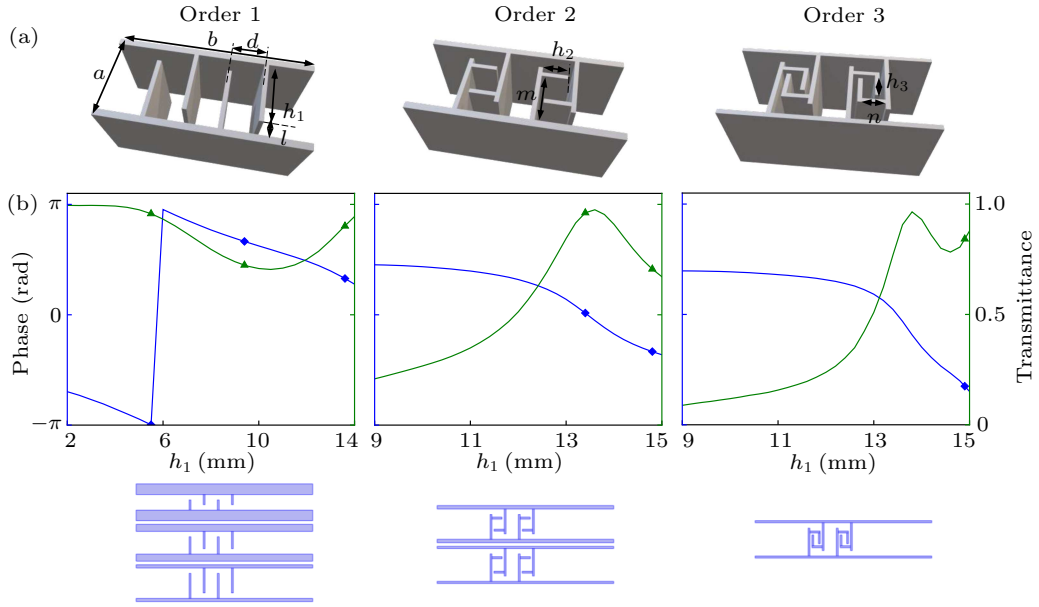


Fig. 2. Geometry analysis of the fractal-inspired hierarchical meta-atoms based on the fretwork frame. (a) Three-dimensional schematic diagram of the meta-atom from order 1 to order 3. (b) Dependence of phase and sound transmittance on the geometry parameter h_1. The six structures selected to construct the metasurface are marked, with a phase interval of $\pi/3$ and transmittance over 0.7.

3. Results and discussion

The numerical simulation is performed by using the coupled modules of Pressure Acoustics and Thermoacoustics in the finite element software (COMSOL Multiphysics). The background is air and the metasurface is made of acrylic plastic (density: 1190 kg/m^3; sound speed: 2750 m/s). The boundaries of background area are set as plane wave radiation condition, and the boundaries of the structure are set as rigid boundary condition. Sound waves at the target incident angle propagate from one side and transmit to another side of the metasurface. The experiments are conducted in an airborne sound measurement system, as depicted in Fig. 3(a). The metasurface sample is 3D-printed by resin and firmly sandwiched between the planar waveguide plates (3-cm air gap between the plates). The continuous sine wave is generated by the function signal generator (Keysight, 33500B Series) and fed to the speaker array consisting of 7 elements through an audio amplifier (Shinco, X-500). A microphone (BSWA-MPA436A, 7-mm diameter) is installed on the electric stepping motor to record the acoustic signal in the 20 cm×20 cm scanning region, with a scanning step of 1 cm in both the x and y directions. The measured signals and incident signals are simultaneously connected to the sound and vibration acquisition card (National Instruments, 9232), for synchronizing the measured phase and referent phase. The enlarged photograph displays the details of one period structure including six meta-atoms with the phase interval of $\pi/3$. The dependence of unidirectional transmission on the propagation direction is demonstrated by measuring the sound pressure fields incident from the forward and backward directions, both in simulations and experiments, as shown in Figs. 3(b) and 3(c). The operating frequency is 4500 Hz and the incident angle is 25°. The black and red arrows represent the incident and transmitted wave, respectively. An apparent difference in sound transmission is revealed between the opposite orientations: the incident wave from the front side is preferentially propagating with high efficiency, whereas from the back side is dramatically reduced due to the multiple reflections. Fairly good agreements are observed between the measured and simulated results. The transmitted energy contrast here is 8 times (9.03 dB), by calculating the ratio of the transmitted acoustic intensity integral within the same area in the forward and backward incident situations.

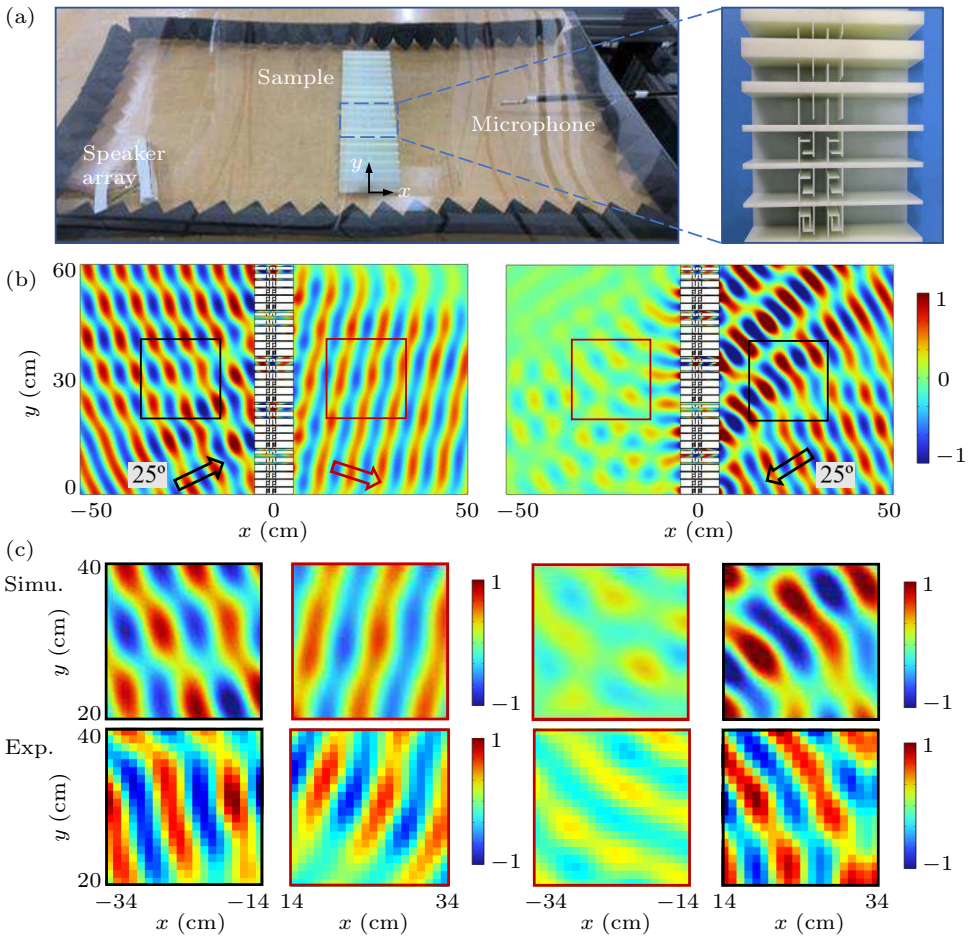


Fig. 3. Dependence of asymmetric transmission on the propagation direction. (a) Photographs of the experimental (Exp.) setup for the airborne sound measurement system and one period structure of the 3D-printed metasurface. (b) Simulated sound pressure fields in the forward and backward incident situations, with the incident angle of 25°. (c) Comparisons between the experimental and simulated (Simu.) pressure fields.

We further quantitatively evaluate the relationships of asymmetric transmission on the incident angle and operating frequency. The transmitted energy contrast with the incident angle from 0° to 50° at 4500 Hz is displayed in Fig. 4(a). The critical angle of the anomalous modulation in our design is calculated to be 21.4°, according to the formula $\theta = \arcsin[1-(\mathrm{d}\Phi/\mathrm{d}x)/k_0]$.[35] Therefore, the energy contrast is inconspicuous if the incident angle is smaller than the critical angle. Conversely, strong asymmetry is expected to appear when the incident angle exceeds the critical angle. The energy contrast over 8 times is acquired within the incident angle from 25° to 50°, agreeing with the theoretical calculation. The larger effective incident angle range could contribute to expanding the applications in practical scenarios where one might aspire to transmit the modulated waveform consisting of different wavevector components, and suppress the undesired noise from different directions. Furthermore, we analyze and compare the energy contrast as a function of frequency range at 4000 Hz–5000 Hz with the incident angles from 5° to 45°, as plotted in Fig. 4(b). The energy contrast remains relatively low over the frequency range for the 5° and 15° oblique incidences. On the contrary, an obvious resonance peak around 4500 Hz is observed for the incident angles of 25°, 35°, and 45°, convincingly verifying the remarkable sound anomalous modulation in the forward and backward propagations.

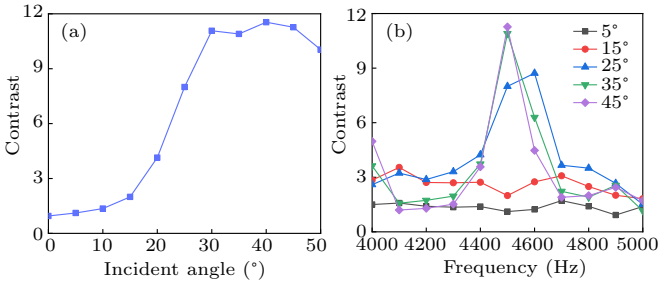


Fig. 4. Characterization of transmitted energy contrast between the forward and backward propagations in simulation. (a) Energy contrast as a function of incident angle within 0°–50° at 4500 Hz. (b) Energy contrast as a function of operating frequency at 4000 Hz–5000 Hz, with different incident angles.

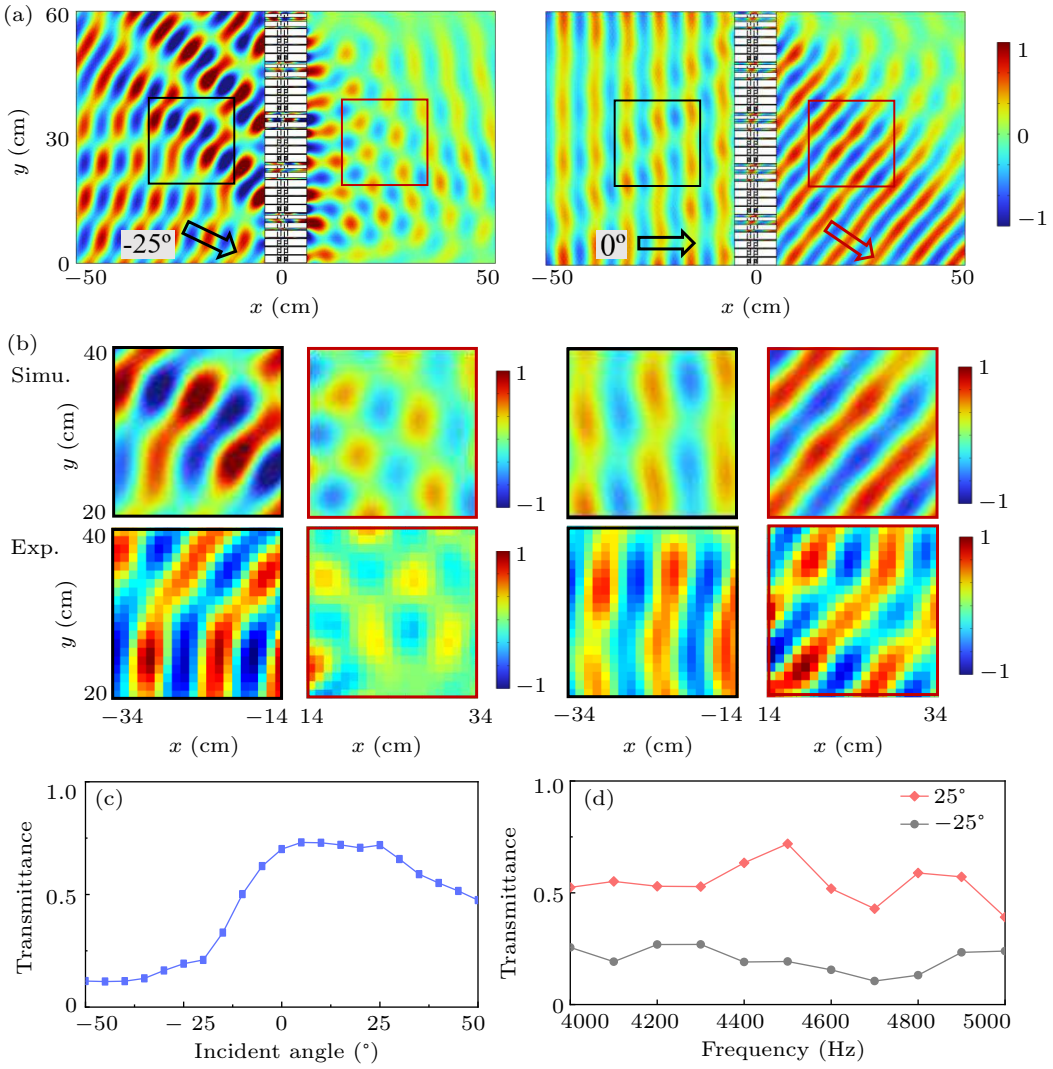


Fig. 5. Dependence of asymmetric transmission on the incident angle from the same propagation side. (a) Simulated pressure fields at −25° and 0°. (b) Comparisons of sound pressure fields in simulations and experiments. (c) Relationship between sound transmittance and incident angle at 4500 Hz. (d) Simulated transmittance at 25° and −25° within the frequency range 4000 Hz–5000 Hz.

In addition to the incidence from the opposite propagation directions of the fractal fretwork metasurface, acoustic asymmetric transmission also occurs between the positive and negative angles when sound wave propagates from the same side. Here we demonstrate the comparison of opposite angles both in the forward propagation as an example, and the unidirectional results are inverse for the backward propagation. Sound pressure fields incident from different angles are shown in Figs. 5(a) and 5(b). In the left panel, it is clearly found that the sound wave at the negative angle -25° is obviously suppressed, distinctly compared with the unhindered propagation at the positive angle 25° [left panel in Figs. 3(b) and 3(c)]. We also present the normalized pressure field at 0° in the right panel, where sound wave vertically impinges to the metasurface and transmits without significant attenuation. The experimental sound fields agree well with the simulated enlarged views. Furthermore, we summarize the relationship between sound transmittance and incident angle at 4500 Hz in Fig. 5(c). The transmittance, calculated as the ratio of transmitted sound intensity with and without the metasurface, is higher than 0.7 for the small incident angle from 0° to 25°. On the contrary, sound wave at -50° to -25° experiences multiple reflections due to the viscosity loss within the metasurface, resulting in the transmittance lower than 0.2. As a result, the transmittances in the cases of 25° and -25° are 0.72 and 0.19, respectively. The gradually increasing of transmittance within -20° to 0° and the dropping within 30° to 50° are mainly attributed to the critical angle and impedance mismatch between the background medium and the metasurface at large incident angle. Moreover, we compare the transmittance at 25° and -25° in the frequency of 4000 Hz–5000 Hz, as plotted in Fig. 5(d). The durative significant difference within the frequency range indicates the effective manipulation between the positive and negative angles in the same propagation direction.

4. Conclusions

In conclusion, we draw inspiration from both the fractal geometry in nature creature and the fretwork frame in ancient culture to design the acoustic subwavelength metasurface, which greatly packs detailed structural features into compact space and produces additional sound propagation path without the scale-up of overall dimensions. We experimentally demonstrated the application of the fractal fretwork metasurface for sound anomalous modulation, and realized the robust and high-contrast asymmetric transmission. Sound wave in the forward direction effectively transmits at positive angle while suffers strong attenuation at negative angle. The propagation of sound wave in the backward direction is exactly opposite to the forward guidance, giving rise to an incident-dependent control to select the on/off state over sound energy flow. In addition, sound transmittance and transmitted energy contrast are quantitatively summarized to analyze the unidirectional transmission under different propagation conditions, involving the incident direction, angle, and frequency. Our proposal may offer a feasible approach for the metasurface design methodology, and possess fascinating prospects in the integration of acoustic devices.

Acknowledgements

Project supported by the National Key Research and Development Program of China (Grant No. 2022YFA1404500), the National Natural Science Foundation of China (Grant Nos. T2222024 and 12034005), the STCSM Science and Technology Innovation Plan of Shanghai Science and Technology Commission (Grant Nos. 20ZR1404200 and 21JC1400300).

References

[1] Mandelbrot B B and Wheeler J A 1983 *Am. J. Phys.* **51** 286
[2] Lakes R 1993 *Nature* **361** 511
[3] Gouyet J F 1997 *Am. J. Phys.* **65** 676
[4] Anazawa M, Ishikawa A, Suzuki T and Tomoyose M 2004 *Physica A* **335** 616
[5] Meyer H V, Dawes T J W, Serrani M, *et al*. 2020 *Nature* **584** 589
[6] Du Q, Yang H, Lv T and Wang X 2013 *Opt. Commun.* **74** 301
[7] Oftadeh R, Haghpanah B, Vella D, Boudaoud A and Vaziri A 2014 *Phys. Rev. Lett.* **113** 104301
[8] Song G Y, Huang B, Dong H Y, Cheng Q and Cui T J 2016 *Sci. Rep.* **6** 35929
[9] Miniaci M, Krushynska A, Gliozzi A S, Kherraz N, Bosia F and Pugno N M 2018 *Phys. Rev. Appl.* **10** 024012
[10] Wu G, Ke Y, Zhang L and Tao M 2022 *Appl. Phys. Express* **15** 014002
[11] Chen Y, Peng R and You Z 2015 *Science* **349** 396
[12] Kim W, Byun J, Kim J K, Choi W Y, Jakobsen K, Jakobsen J, Lee D Y and Cho K J 2019 *Sci. Robot.* **4** eaay3493
[13] Walker A and Stankovic T 2022 *Commun. Mater.* **3** 4
[14] Li Y, Liang B, Gu Z M, Zou X Y and Cheng J C 2013 *Sci. Rep.* **3** 2546
[15] Xie Y, Popa B I, Zigoneanu L and Cummer S A 2013 *Phys. Rev. Lett.* **110** 175501
[16] Cheng Y, Zhou C, Yuan B G, Wu D J, Wei Q and Liu X J 2015 *Nat. Mater.* **14** 1013
[17] Jeon G J and Oh J H 2021 *Phys. Rev. E* **103** 012212
[18] He J J, Jiang X, Ta D A and Wang W Q 2020 *Appl. Phys. Lett.* **117** 091901
[19] Yu G, Qiu Y, Li Y, Wang X and Wang N 2021 *Phys. Rev. Appl.* **15** 064064
[20] Zhou P, Jia H, Bi Y, Liao B, Yang Y, Yan K, Zhang J and Yang J 2022 *Phys. Rev. Appl.* **18** 014050
[21] Melde K, Mark A G, Qiu T and Fischer P 2016 *Nature* **537** 518
[22] Zhu Y and Assouar B 2019 *Phys. Rev. Mater.* **3** 045201
[23] Zhu J, Christensen J, Jung J, Martin-Moreno L, Yin X, Fok L, Zhang X and Garcia-Vidal F J 2011 *Nat. Phys.* **7** 52
[24] Shen Y X, Peng Y G, Cai F, Huang K, Zhao D G, Qiu C W, Zheng H and Zhu X F 2019 *Nat. Commun.* **10** 3411
[25] Chen A, Zhao X, Yang Z, Anderson S and Zhang X 2022 *Phys. Rev. Appl.* **18** 064057
[26] He J J, Zhou Z L, Zhang C X, Zheng Y, Li Y, Li Y, Jiang X and Ta D A 2022 *Appl. Phys. Lett.* **120** 191701
[27] Zhou Z L, Huang S B, Li D T, Zhu J and Li Y 2022 *Natl. Sci. Rev.* **9** nwab171
[28] Zhang S, Zhang Y, Guo Y J, Leng Y H, Feng W and Cao W W 2016 *Phys. Rev. Appl.* **5** 034006
[29] Wu L T, Zhang C, Ke J C, Cheng Q, Cui T J and Jing Y 2019 *Sci. Bull.* **64** 808

[30] Gu Z M, Gao H, Cao P C, Liu T, Zhu X F and Zhu J 2021 *Phys. Rev. Appl.* **16** 057001
[31] Wang R and Yang F B 2022 *Appl. Phys. Express* **15** 104003
[32] Fleury R, Sounas D L, Sieck C F, Haberman M R and Alù A 2014 *Science* **343** 516
[33] Popa B I and Cummer S A 2014 *Nat. Commun.* **5** 3398
[34] Devaux T, Tournat V, Richoux O and Pagneux V 2015 *Phys. Rev. Lett.* **115** 234301
[35] Li Y, Shen C, Xie Y, Li J, Wang W, Cummer S A and Jing Y 2017 *Phys. Rev. Lett.* **119** 035501
[36] Xie B, Cheng H, Tang K, Liu Z, Chen S and Tian J 2017 *Phys. Rev. Appl.* **7** 024010
[37] Ju F, Tian Y, ChengY and Liu X 2018 *Appl. Phys. Lett.* **113** 121901
[38] Zhu Y F, Zou X Y, Liang B and Cheng J C 2015 *Appl. Phys. Lett.* **107** 113501
[39] Zhu J, Zhu X F, Yin X B, Wang Y and Zhang X 2020 *Phys. Rev. Appl.* **13** 041001
[40] Xia J P, Zhang X T, Sun H X, Yuan S Q, Qian J and Ge Y 2018 *Phys. Rev. Appl.* **10** 014016
[41] Zuo S, Tian Y, Cheng Y, Deng M, Hu N and Liu X 2019 *Phys. Rev. Mater.* **3** 065204
[42] Zhu J, Zhu X, Yin X, Wang Y and Zhang X 2020 *Phys. Rev. Appl.* **13** 041001
[43] Zhou Z, Jia B, Wang N, Wang X and Li Y 2023 *Phys. Rev. Lett.* **130** 116101
[44] Yu N, Genevet P, Kats M A, Aieta F, Tetienne J P, Capasso F and Gaburro Z 2011 *Science* **334** 333
[45] Xie Y, Wang W, Chen H, Konneker A, Popa B I and Cummer S A 2014 *Nat. Commun.* **5** 5553
[46] Mei J and Wu Y 2014 *New J. Phys.* **16** 123007
[47] Qian E, Fu Y, Xu Y and Chen H 2016 *Europhys. Lett.* **114** 34003